REPORT DOCUMENTATION PAGE

Form Approved
OMB No. 0704-0188

PLEASE DO NOT RETURN YOUR FORM TO THE ABOVE ORGANIZATION.

1. REPORT DATE *(DD-MM-YYYY)*	2. REPORT TYPE	3. DATES COVERED *(From - To)*
09-10-2009	Journal Article	

4. TITLE AND SUBTITLE
Internal Gravity Waves in the Strait of Luzon: Dispersion Studies Using Fourier and Continuous Wavelet Transforms

5a. CONTRACT NUMBER

5b. GRANT NUMBER

5c. PROGRAM ELEMENT NUMBER
0602435N

6. AUTHOR(S)
Jim Hawkins, Alex C. Warn-Varnas

5d. PROJECT NUMBER

5e. TASK NUMBER

5f. WORK UNIT NUMBER
73-6838-A7-5

7. PERFORMING ORGANIZATION NAME(S) AND ADDRESS(ES)
Naval Research Laboratory
Oceanography Division
Stennis Space Center, MS 39529-5004

8. PERFORMING ORGANIZATION REPORT NUMBER
NRL/JA/7320-08-8340

9. SPONSORING/MONITORING AGENCY NAME(S) AND ADDRESS(ES)
Office of Naval Research
800 N. Quincy St.
Arlington, VA 22217-5660

10. SPONSOR/MONITOR'S ACRONYM(S)
ONR

11. SPONSOR/MONITOR'S REPORT NUMBER(S)

12. DISTRIBUTION/AVAILABILITY STATEMENT
Approved for public release, distribution is unlimited.

13. SUPPLEMENTARY NOTES

14. ABSTRACT
Investigation of the dynamics of internal gravity waves often includes the interrelationship between wave amplitudes, wave speeds, and wavelengths. These relationships are commonly thought of as dispersion relations. Because internal gravity waves are the result of nonlinear dynamics dispersion relations are a challenge to obtain in a quantitative sense. Model data for internal gravity waves in the Strait of Luzon are examined using Fourier and continuous wavelet transforms. Dispersion is qualitatively evident in the results and the investigation is extended to include quantitative assessment of the dispersion. The results are compared to results from Korteweg D'Vries theory. Good agreement is obtained for dispersion estimates using wavelet analysis and those from KdV theory.

15. SUBJECT TERMS
internal waves, synthetic aperture radar, FFT

16. SECURITY CLASSIFICATION OF:			17. LIMITATION OF ABSTRACT	18. NUMBER OF PAGES	19a. NAME OF RESPONSIBLE PERSON
a. REPORT	b. ABSTRACT	c. THIS PAGE			Alex Warn-Varnas
Unclassified	Unclassified	Unclassified	UL	10	19b. TELEPHONE NUMBER *(Include area code)* 228-688-5223

Eur. Phys. J. Special Topics 174, 227–236 (2009)

DOI: 10.1140/epjst/e2009-01103-x

THE EUROPEAN PHYSICAL JOURNAL SPECIAL TOPICS

Regular Article

Internal gravity waves in the Strait of Luzon: Dispersion studies using Fourier and continuous wavelet transforms

J.A. Hawkins[1,a] and A. Warn-Varnas[2]

[1] Planning Systems Inc., Slidell, 70458, LA, USA
[2] Naval Research Laboratory, Stennis, MS, USA

Abstract. Investigation of the dynamics of internal gravity waves often includes the interrelationship between wave amplitudes, wave speeds, and wavelengths. These relationships are commonly thought of as dispersion relations. Because internal gravity waves are the result of nonlinear dynamics dispersion relations are a challenge to obtain in a quantitative sense. Model data for internal gravity waves in the Strait of Luzon are examined using Fourier and continuous wavelet transforms. Dispersion is qualitatively evident in the results and the investigation is extended to include quantitative assessment of the dispersion. The results are compared to results from Korteweg D'Vries theory. Good agreement is obtained for dispersion estimates using wavelet analysis and those from KdV theory.

1 Background

Internal waves (IWs) occur throughout the world's oceans and seas. Well known examples include IWs in the Mediterranean Sea generated in the nearby Strait of Gibraltar, those found in the Sulu Sea and in the South China Sea. The subject of the investigation here is IWs generated in the Luzon Strait and propagating through the northeast area of the South China Sea. Figure 1 shows examples of these IWs as synthetic aperture radar (SAR) images (these images were obtained from the University of Delaware's internal wave atlas, `http://atlas.cms.udel.edu/`).

Internal waves arise as the result of stratified tidal flow over topography. For example, flow over a submarine sill may induce a depression (or rise) in the thermocline which steepens as a result of finite amplitude and eventually may break into solitary wave packets through dispersion. The result is that an internal wave may change dramatically over the course of its generation and propagation [1,3]. A qualitative description of IW dispersion in the Luzon Strait is contained in a previous work of the authors [4].

While IWs share many attributes of more evident surface waves they differ in some important aspects. For example, surface waves reach large amplitudes at the sea surface and may crest and break. In contrast IW's maximum amplitudes occur at or near the thermocline many tens of meters below the ocean surface. In fact, surfacial evidence of IWs can be subtle if detectable at all. Nevertheless, alternating bright and dark concentric arcs caused by convergence and divergence of IW currents can appear as a perturbation of sea surface roughness as observed in the previous SAR images.

Quantifying internal wave changes over the course of its generation and propagation typically focuses on the size, speed, and separation within the IW packet of its component solitary waves. These effects are broadly categorized as dispersion. Measuring IW dispersion is not as straight forward a problem as in the case of linear wave propagation due to the underlying nonlinear

[a] e-mail: `jhawkins@plansys.com`

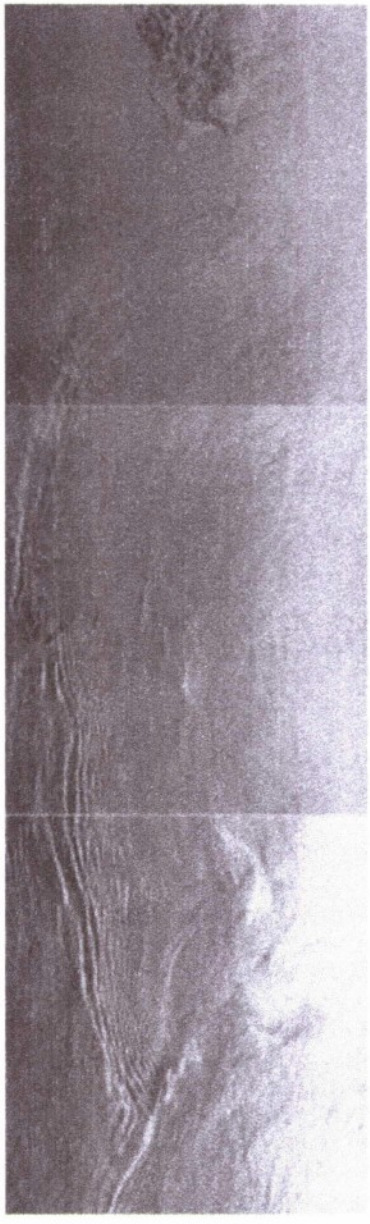

Fig. 1. Internal gravity waves as seen in SAR images. Taiwan is at the upper edge of the image. (From the University of Delaware's internal wave atlas, `http://atlas.cms.udel.edu/`.)

physics of internal waves. As such, the application of the usual tools for analysis, for example Fourier techniques, fall short in some respects in trying to quantify dispersion. Wavelet analysis addresses many of the problems with Fourier techniques, however wavelet analysis is essentially a linear tool and thus is constrained in some sense as Fourier techniques. In fact internal waves retain a good deal of 'linear' information that is elucidated with the Fourier and wavelet analysis techniques described in this paper.

The effort described here represents an extension of the earlier work of the authors [4]. We hope to more fully describe, in a quantitative sense, the effects arising from dispersion. The generation and propagation is briefly described in the following section. In Section 3 the changes

that arise in the evolution of internal waves are described in a qualitative sense using illustrations from model results. Section 3 presents a general summary of Fourier and Wavelet analysis applied to internal waves. This represents something of a review and the reader is referred to [4] for more details. Section 4 deals with quantitative estimation of dispersion occurring during internal wave development. Moreover, the results are compared to an approximate analytic formulation for dispersion based on the Korteweg d'Vries equation. In the concluding section the results are summarized and commented upon.

2 Model and data

A sill spans the Strait of Luzon from Taiwan in the north, south towards the Philippines (see Fig. 1). Flow over the sill generates internal depressions which evolve into internal solitary waves. A 2D non-hydrostatic Boussinesq model with rigid lid approximation is used to model internal waves in the strait [5,6]. Results from this model study are analyzed in the present work.

The topography of the sill is approximated by an analytic function and the tidal forcing is obtained from the Oregon State University database and the Naval Coastal Prediction Model (NCOM). Initial continuously varying, density profiles are generated with analytic functions based on data from the area (NCOM). Results from the model are shown in Figure 2.

A complex density field (Fig. 2) is obtained in a vertical slice of the water column surrounding the sill after 70 hours of simulation time. The vertical axis is depth in meters and the horizontal axis is distance in kilometers away from the sill. The origin is taken to be the summit of the eastern sill. Note that the aspect ratio is very large which allows easy elucidation of the internal wave field.

Internal wave packets can be identified at roughly -200, -500 and -600 km with perhaps a smaller packet located between -300 and -400 km. A depression can be seen (particularly at about 1000 m depth) just to the east of -100 km. Taken together the depression and the three packets provide snapshots of the internal wave over the course of its existence. In other words, the internal waves shown here can be thought of in terms of an initial depression which evolves into a series of tightly spaced solitary waves, growing in size initially but eventually diminishing as the packets approach the China coast. The apparent diminution of the signal after 72 hours is thought to be a numerical artifact and not predictive.

In the next section, the inception and development of the internal wave packet is more closely examined.

3 Dispersion

The approach to describing dispersion is twofold. First we outline the qualitative description of dispersion and follow with a more quantitative approach.

3.1 Qualitative description of dispersion

The evolution of internal waves described in the previous section can be more fully seen by examining a single isopycnal surface over a series of time intervals (see Fig. 3).

The isopycnal surface illustrated in Fig. 3 evolves over the course of 88 hours of simulation in 2 hour increments. The amplitude of the oscillations are normalized for relative comparison. For the first 24 hours the isopycnal is relatively quiescent with a depression developing at the eastern edge of the domain. The depression that emerges after 20 hours develops into an internal wave packet by 36 hours. This initial packet, while well developed, is not thought to be representative of the ensuing internal waves. Hence, later internal waves will be used for analysis.

Note the pattern of initial depression, subsequent steepening at the 'front' of the internal wave packet, eventual breakdown into a series of internal solitary waves and finally diminution

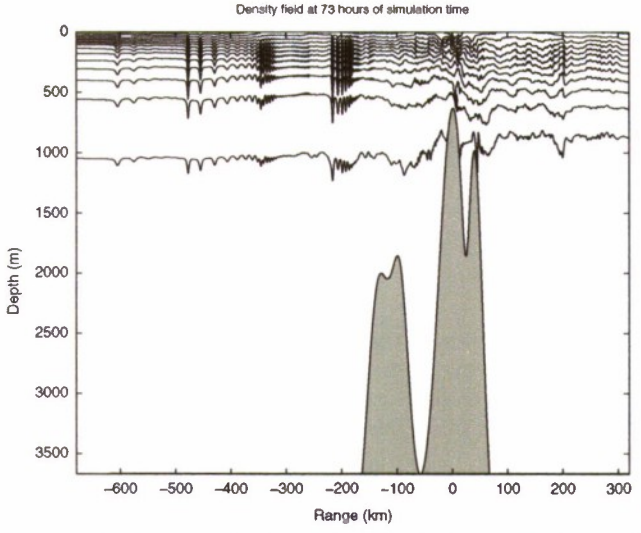

Fig. 2. Image of isopycnal surfaces for model simulation after 72 hours. The internal waves are generated at the 'eastern' sill (shaded area).

and disappearance of most of the oscillations in the packet. The description of this behavior is broadly described as dispersion. Quantifying this behavior is the goal here.

3.2 Quantitative description of dispersion

Two related but unique techniques are applied to the internal waves described in the previous section. The first is the Fourier transform implemented with the fast Fourier transform (FFT). The second is the continuous wavelet transform. First the FFT is considered.

The Fourier decomposition of an individual internal wave packet at three intervals is pictured in Fig. 4 (the components are computed using FFT routines from MATLAB [9]). From bottom to top panel the intervals shown are the packet at 36, 60, and 84 hours. The internal wave packets are taken from the second set of solitary waves seen in Fig. 3. The right side panels show the internal wave packet analyzed and the left panels show the Fourier spectrum as a function of wavenumber. Note that the spectral amplitudes are multiplied by the frequency in order to emphasize the low frequency components of interest. The limits of the spectrum shown includes the components between the Brunt-Vaisala frequency and the Coriolis frequency. These components are of importance because wavelengths associated with propagating internal wave modes fall between these limits [7]. For example, IWs of 5–20 km travelling roughly 2 m/s will have periods on the order of about an hour compared to a Brunt-Vaisala of several cycles per hour and the Coriolis frequency with a period of 35 hours at latitude 20° N.

In Fig. 4 the increase in internal wave modes is apparent. The growth in the number and amplitude of the internal wave modes, those near 0.1 and 0.2 km^{-1}, rises dramatically from 36 to 84 hours.

While the growth in number and amplitude of internal waves modes is apparent, the exact nature of the growth is nevertheless obscure. It would be advantageous to have spatial localization of the components. Researchers have, among an array of techniques, employed amplitude versus speed and amplitude versus wavelength observations to characterize the dispersion of IWs (see for example Varnas et al. [6]). Here we propose to exploit the wavelet transform to estimate dispersion.

The wavelet transform has proven to be useful in analyzing a non-stationary processes, one whose spatial and temporal characteristics vary over time (for example see [8]). Roughly speaking, the wavelet transform can be thought of as a windowed FFT. That is, if a window

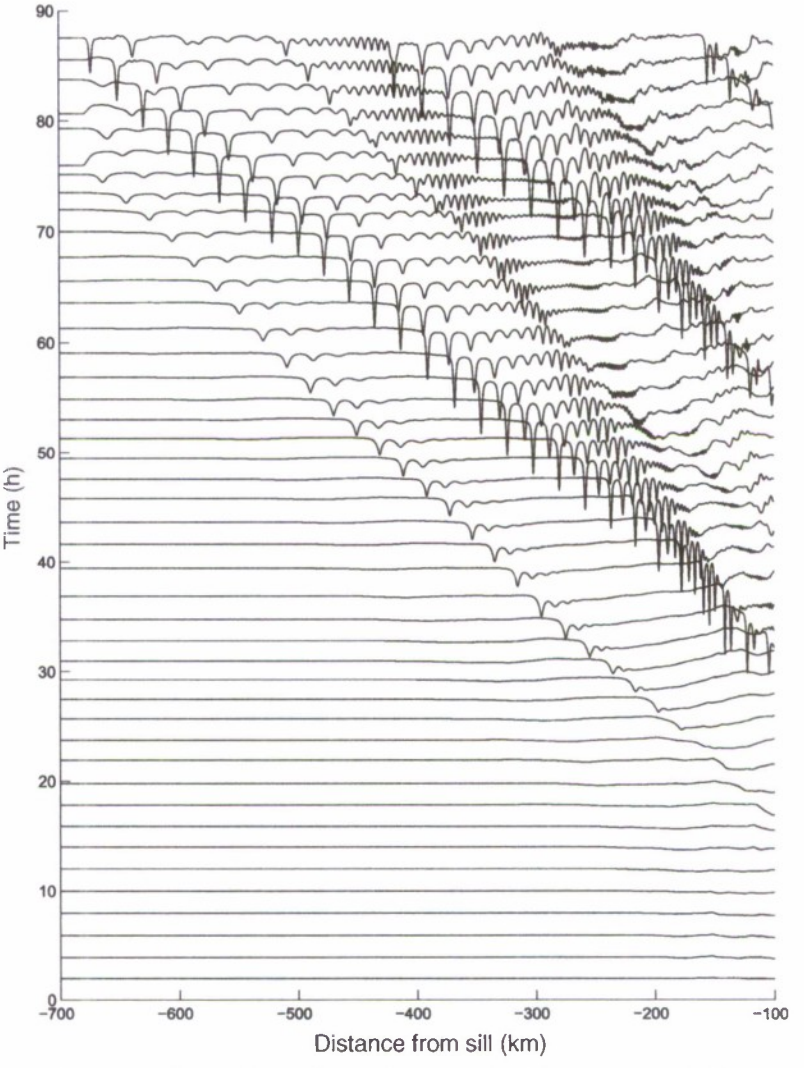

Fig. 3. The development and evolution of internal wave packet for an isopycnal at 150 m depth shown over 86 hours in two hour increments beginning at the bottom and proceeding upward. Scaling is normalized to emphasize relative size.

were to be slid along the isopycnal waveform and the resulting components calculated from the windowed segment, then the spatial occurrence of components could be estimated. The windowed Fourier transform itself can be used to do this (see for example the spectrogram function [9]), however the technique is often complicated by edge effects from the 'window'. The wavelet transform represents an improvement over the windowed FFT in that the sliding window is now a smooth wavelet (in the case of a continuous wavelet). In this sense the wavelet transform provides a means to circumvent complicating edge effects and preserves the local information of Fourier components [8]. Here the Morlet wavelet is used which has an analytic connection to Fourier wavelengths. A good description of wavelet analysis including the continuous wavelet transform can be found in the literature (see, for example, [10] and [11]).

Note that the continuous wavelet transform does not yield a set of orthogonal wavelet bases such as one would obtain from discrete wavelet analysis. In fact there is redundancy in the wavelet components derived from continuous wavelet analysis which prevents easy identification of a small number of wavelet components which adequately represent a signal. On the

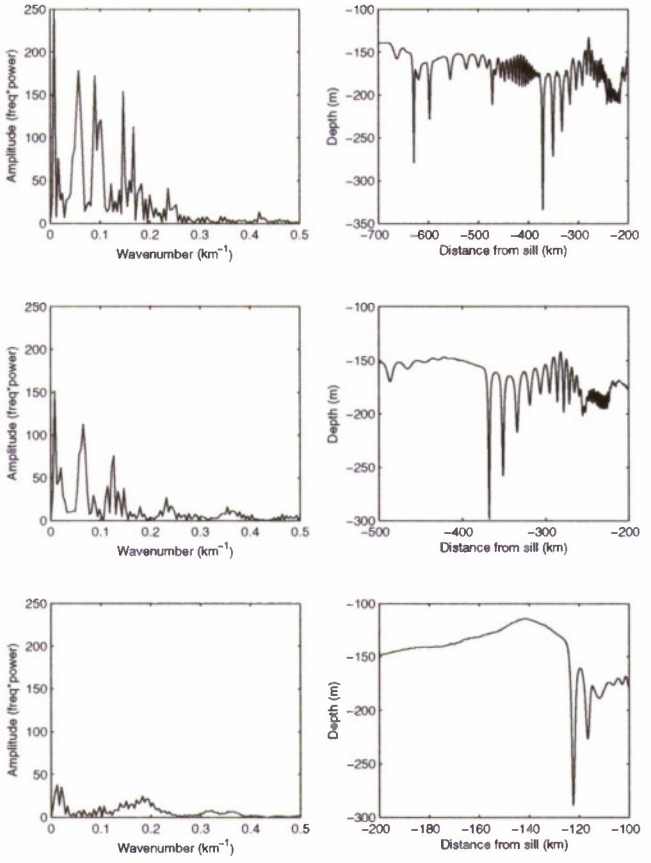

Fig. 4. Power spectral density (power is multiplied by frequency). The times series are taken from simulation time intervals 36 h, 60 h and 84 h (proceeding from the lowermost to uppermost panel). Note the growth in components with wavenumbers less than $0.2\,\mathrm{km}^{-1}$.

other hand, continuous wavelet transforms allow the smooth depiction of changes over time. A broader treatment would include the use of a wide range of continuous and discrete wavelet techniques. For conciseness, we have restricted our analysis to the continuous wavelet transform using the Morlet wavelet, however, the analysis is completely general.

The evolution of the three packets introduced above is evident in their associated wavelet spectrum (Fig. 5). The darker gray areas within the left side panels shows the intensity (dark gray high amplitude, light gray low) and wavelength of the constitutive components of the internal wave packets. As such the development and evolution of the components is evident. In the earliest interval the wavelength is near 5 km. As the internal wave packet propagates the dominant component increases in length (near 20 km) and intensity. Finally the components diminish significantly between −600 km and −700 km in the uppermost panel. Note that the components of the following wave packet is similar to that in the mid panel.

While the wavelet transform gives a graphic picture of the evolving nature of Fourier components, it also provides a means to calculating an estimate of the dispersion relation. This represents a substantial extension to the qualitative depiction of IW dispersion. In the next section the method to obtain an estimate of the dispersion relation is presented.

4 Dispersion estimates using wavelet components

Each wavelet component arising from the Morlet wavelet transform can be associated with a Fourier wavelength [8]. The wavelet spectrum (Fig. 5) graphically localizes the occurrence

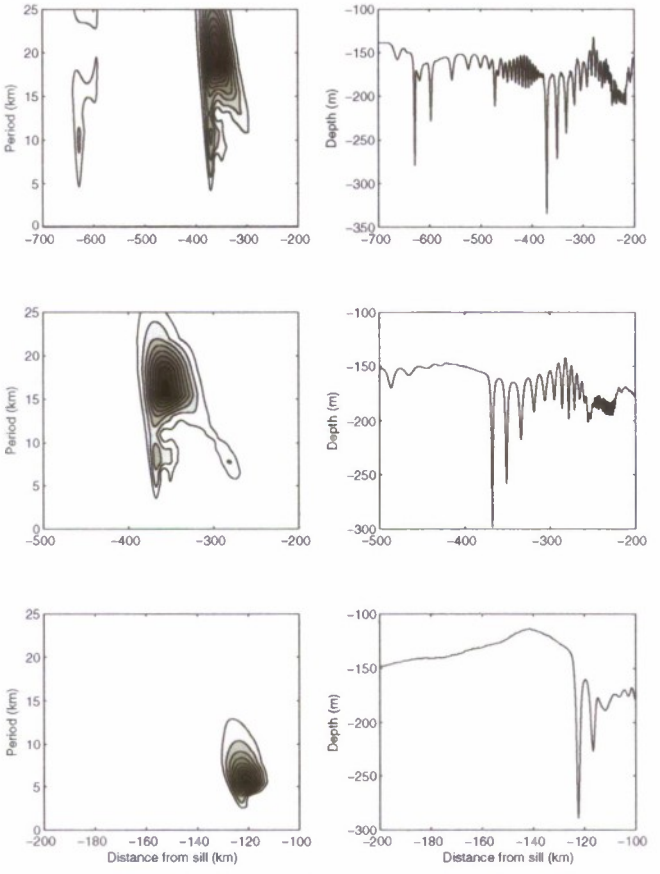

Fig. 5. Wavelet spectrum at three times. The times series are taken from simulation time intervals 36 h, 60 h and 84 h (proceeding from the lowermost to uppermost panel). The dominant wavelength grows from just over 5 km to about 20 km.

of each of the Fourier components. Moreover, the peaks in the wavelet spectrum have a 3 dimensional aspect, there is a rise due to amplitude and a spread in two directions, range and wavelength. In this regard the wavelet spectrum is analogous to a ridge or rise in a topographic map. In fact, each component has a peak at each interval corresponding to the peak in the components amplitude. Following the peak for each component over time provides a 'track' for that component. By noting the time and location of the peak the 'phase speed' of that component can be estimated. The analysis here closely follows that of Meyers [12] where cross sections at three times encompassing the internal wave packet are analyzed. This Lagrangian approach is in contrast to a strictly Eulerian approach as one might obtain using a time series of measured temperature values. However the assumption is that there no appreciable error is incurred during each 'snapshot'.

The largest amplitude IWs are often found at a depth where the maximum of the density gradient occurs. An isopycnal surface near this level is depicted at three time intervals, 36, 42 and 48 hours, in the upper panel of Fig. 6. The lower panel contains the wavelet spectrum for each interval and an associated 'spine' which localizes the peaks for a series of wavelengths. Notice that the spine changes over the time intervals with the peaks nearly at the identical range at 36 hours while at 42 hours the longer wavelengths have travelled considerably farther. The implication is clearly that longer wavelengths have greater 'phase' speed.

The phase speed can be computed explicitly by assuming a linear speed for each wavelength peak. For example, by tracking the location of the 10 km wavelet component over

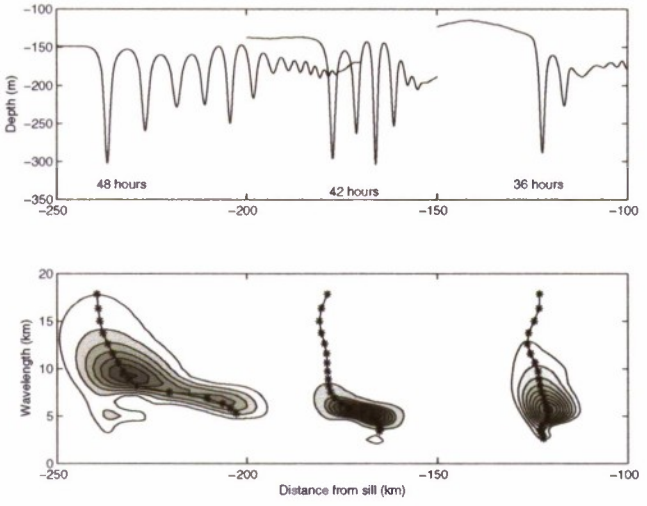

Fig. 6. Isopycnal surface at three simulation intervals (proceeding right to left): 36, 42, and 48 hours (upper panel). Corresponding wavelet spectrum with wavelength peaks shown as 'spine' (lower panel).

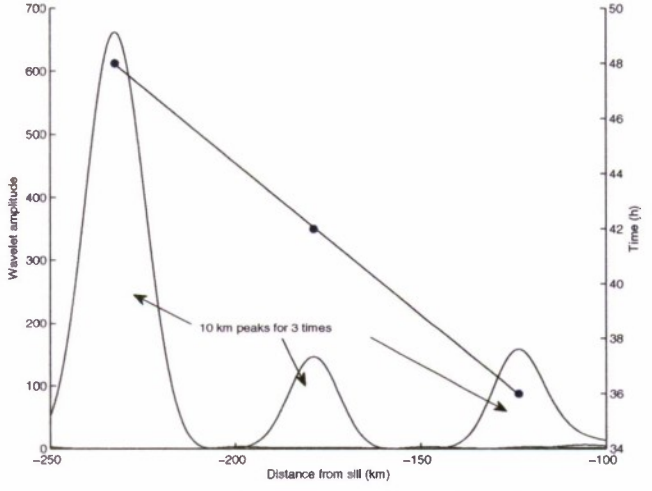

Fig. 7. Location of the peak power and the associated linear fit for the 10 km wavelet component at 3 times.

3 times (Fig. 7) an approximate speed can be computed (it is noted that only 3 intervals are used in computing the phase speeds, nevertheless we have found that the IW packet changes slowly over 12 hours and only small errors are incurred). The process is repeated for several wavelengths thereby yielding a phase speed versus wavelength comparison.

The results of the phase speed estimation are then arranged to form a dispersion diagram. It is noted that the linear estimate of phase speed is better for some components than for others. For longer wavelengths, near 10 km and above, the spine (Fig. 6) tends to 'bend' to the left. For these components the linear approximation works well. For shorter wavelengths the fit is less good. It is speculated that more complicated physical processes are occurring near the 'tail' of the IWs (see for example, the portion of the IW at 48 h near −200 km in Fig. 6). Nevertheless, the analysis shows that for a reasonable range of wavelengths the phase speed of each component is well modeled by its linear approximation.

The resulting dispersion curve is displayed (Fig. 8) along with curves derived from Korteweg D'Vries theory. We recognize that KdV theory describes a two-layer model and the IWs under

investigation occur in a continuously varying density field. Nevertheless, the IWs described here are located near a depth where the gradient is a maximum. Similarly, the two-layer model can be thought of as a profile where the density 'jumps' from one value to another. In this sense the dispersion results from KdV represent a limiting case and provide reasonable boundaries for comparison.

Apel and Gonzalez [7] have transcribed a dispersion relationship for linear dispersive and nonlinear dispersive phase speeds used here. The formula for phase speed c_p is as follows:

$$c_p = c_0(1 - \gamma k_l^2 + 2\alpha A/3), \tag{1}$$

where c_0 is the linear phase speed, γ is given by,

$$\gamma = \frac{h_2 h_1}{6}, \tag{2}$$

where h_2 and h_1 are the upper and lower layer depths respectively, α is given by,

$$\alpha = \frac{3}{2}\frac{h_2 - h_1}{h_2 h_1} \tag{3}$$

A is solitary wave amplitude and the linear sound speed c_0 is estimated [1,2] as

$$c_0^2 = \delta_\rho g \frac{h_1 h_2}{h_1 + h_2}, \tag{4}$$

where $\delta_g = (\rho_2 - \rho_1)/\rho_2$ is the difference between average densities in the upper and lower layer. The above relations require specifying h_1, h_2, and A. While there is some freedom in these choices (see Table 1) the requirement that the isopycnal surface be near the maximum gradient forced the choice of the upper layer to be near $h_1 = 150$ m. Likewise the amplitude A was chosen to be 100 m, a value observed in the region [13].

Table 1. Table of h_1 and related values.

h_1 m	c_0	γ	α
125	1.8	73750	0.012
150	1.9	87875	0.010
175	1.9	101790	0.008

Figure 8 shows dispersion results as calculated from the above wavelet analysis for two model runs. Case A is the result for the model shown in Fig. 2. This case is tuned to describe IWs recorded in the Luzon Strait and propagating into the South China Sea [6]. Another case (Case B), a variant of the Luzon Strait model is included as an additional example [6]. Note that the dispersion results for Case B, while slightly different, fall within the bounds of the KdV results and are reasonably similar to Case A. The lower curve is the KdV dispersion relation excluding finite amplitude ($\alpha = 0$), and the upper curve includes both dispersion and nonlinearity. Clearly the wavelet calculations compare favorably fall within the bounds of the KdV curves. Consequently, it can be asserted that the physics of the internal wave simulation discussed here is closely modeled by KdV theory.

5 Summary

Modeled results for internal gravity waves in the Strait of Luzon have been analyzed using Fourier and wavelet transforms. A qualitative description of the enception and development of IWs in the Luzon Strait has been undertaken previously by the authors [4]. The aim of the

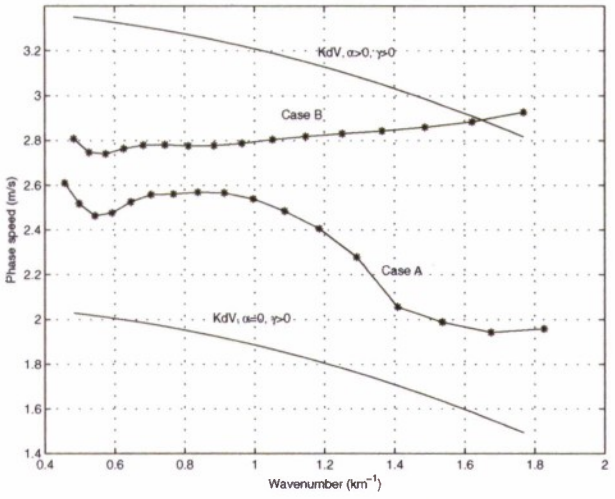

Fig. 8. Estimate of phase speed for wavelengths derived from wavelet analysis (solid line with stars). The dispersion curves from KdV theory are shown with nonlinearity (upper solid curve) and without nonlinearity (lower solid curve).

current analysis is to extend this discussion and quantitatively describe the evolution of internal wave packets over the duration of their existence.

The qualitative evidence of dispersion is vividly demonstrated, calculations using the peaks of the wavelet spectrum are shown to fall within the bounds of KdV theory. In conclusion wavelet analysis provides a good means of assessing agreement between models and theory (in this case KdV theory). Furthermore, it is likely the same comparisons can be employed with due care to field data. This provides a means to tie model data, theory and field data together quantitatively.

References

1. K.R. Helfrich, W.K. Melville, Annu. Rev. Fluid Mech. **38**, 395 (2006)
2. T. Gerkema, Ph.D. thesis, Utrecht University, 1994
3. J.R. Apel, Am. Met. Soc. **33**, 2247 (2003)
4. J.A. Hawkins, A. Warn-Varnas, I. Christov, in *Nonlinear Time Series Analysis in the Geosciences*, edited by R.V. Donner, S.M. Barbosa (Springer, Berlin, 2008), pp. 223–244
5. K.G. Lamb, J. Geo. Res. **99**, 848 (1994)
6. A.W. Varna, J. Hawkins, K. Lamb, S. Piacsek, S. Chin-Bing, D. King, G. Burgos, J. Ocean Modelling (in review)
7. J.R. Apel, F.I. Gonzalez, J. Geophys. Res. **88**, 4459 (1983)
8. C. Torrence, G.P. Compo, Bull. Am. Met. Soc. **79**, 61 (1998)
9. Matlab: Signal Processing Toolbox, Version 6, The MathWorks, Inc. (2002)
10. P. Kumar, E. Foufoula-Georgiou, in *Wavelets in Geophysics*, edited by E. Foufoula-Georgiou, P. Kumar (Academic Press, San Diego, 1994), pp. 1–45
11. L.H. Kantha, C.A. Clayson, in *Numerical Models of Oceans and Oceanic Processes*, edited by L.H. Kantha, C.A. Clayson (Academic Press, San Diego, 2000), pp. 786–818
12. S.D. Meyers, B.G. Kelly, J. O'Brien, Monthly Weather Rev. **121**, 2858 (1993)
13. T.F. Duda, J.F. Lynch, A.E. Newhall, L. Wu, C.-S. Chu, IEEE J. Oceanic Eng. **29**, 1264 (2004)